Morphogenesis of termite mounds

Samuel A. Ocko[a,1], Alexander Heyde[b,1], and L. Mahadevan[b,c,d,e,2]

[a]Department of Applied Physics, Stanford University, Stanford, CA 94305; [b]Department of Organismic and Evolutionary Biology, Harvard University, Cambridge, MA 02138; [c]Paulson School of Engineering and Applied Sciences, Harvard University, Cambridge, MA 02138; [d]Department of Physics, Harvard University, Cambridge, MA 02138; and [e]Kavli Institute for Bionano Science and Technology, Harvard University, Cambridge, MA 02138

Edited by Simon A. Levin, Princeton University, Princeton, NJ, and approved December 17, 2018 (received for review November 7, 2018)

Several species of millimetric-sized termites across Africa, Asia, Australia, and South America collectively construct large, meter-sized, porous mound structures that serve to regulate mound temperature, humidity, and gas concentrations. These mounds display varied yet distinctive morphologies that range widely in size and shape. To explain this morphological diversity, we introduce a mathematical model that couples environmental physics to insect behavior: The advection and diffusion of heat and pheromones through a porous medium are modified by the mound geometry and, in turn, modify that geometry through a minimal characterization of termite behavior. Our model captures the range of naturally observed mound shapes in terms of a minimal set of dimensionless parameters and makes testable hypotheses for the response of mound morphology to external temperature oscillations and internal odors. Our approach also suggests mechanisms by which evolutionary changes in odor production rate and construction behavior coupled to simple physical laws can alter the characteristic mound morphology of termites.

termite mound | animal architecture | niche construction | convection | porous media

Termites are highly eusocial insects, and the large, often elaborate mounds of mound-building termite species protect the colony and internal nest, while providing responsive control over their microenvironment (1, 2). The complex, porous networks that colonies construct within termite mounds help to regulate gas flow, pheromone dispersion, and humidity, which need to be maintained for the specialized purposes of brooding and cultivating the fungal species on which they feed (3, 4). The sculpted morphology of a termite mound is frequently characteristic of the species or genus, being generally conserved within a given species and geography, but strikingly variable across species and environments (Fig. 1) (1). For example, the genus *Amitermes* builds colossal wedge-shaped mounds with a primary axis oriented north–south, a consistent directionality that gives them the common name "compass termites," allowing the internal mound temperature to rapidly increase in the morning but avoid overheating at midday (5). In contrast, the mounds of *Cubitermes* are tall and narrow, while the mounds of *Cornitermes* are small and compact (6). It is thought that these dramatically different mound sizes and shapes allow termites to adapt to their particular environments, but there has been little in terms of quantitative evidence to corroborate this.

Part of the reason for this may be that the physiological ramifications of termite mounds have only recently been clarified. Direct measurement of diurnal variations in flow through the mounds of *Odontotermes obesus* and *Macrotermes michaelseni* shows that a simple combination of geometry, porosity, and heterogeneous thermal mass allows mounds to use diurnal thermal oscillations for another purpose: ventilation, to remove humidity and carbon dioxide from the nest (7, 8). To ensure successful ventilation in different environments, it is crucial that termites construct their mounds in coordination with their surrounding conditions. Even between colonies of the same species, some termites can adapt the morphology of their mound to fit the local environment; *Macrotermes bellicosus* constructs thin-walled, cathedral-shaped mounds in open savannas, for example, but thick-walled, dome-shaped mounds in forested areas (2).

Altogether, the impressive scale and adaptability of termite mounds begs the question of the mechanism by which they are created and maintained. In the absence of a centralized control system or coordinating individual, these elaborate but conserved mound morphologies result from the collective behavior of termites acting only on their perception of local conditions within the mound (9). Mound morphogenesis is thus an extreme exemplar of self-organized animal architecture, where global-scale collective patterns emerge from locally driven individual behaviors, termed "stigmergy" (10–12). Attempts to quantify these processes typically focus on microscopic agent-based models that simulate the behavior of a multitude of organisms computationally (12–16). But since environmental factors, such as temperature and humidity, and sensory stimuli, including pheromone concentrations, vary over slow time scales but long length scales, a natural question is that of an effective description on these scales.

The precise biological mechanism by which termite construction behavior and mound morphology are coupled is not yet fully understood, but a sizable literature of past work typically assumes the existence of some information-carrying field of odor particles, such as secreted pheromones or metabolic gases. Proposed mechanisms can be roughly divided into two broad categories: the secretion of a templating odor at the nest that undergoes diffusion and advection globally throughout the mound, and the local deposition of a building pheromone in deposited soil pellets that promote further deposition nearby (17–19). Templating can assist in the formation of large-scale structures, and there exists some experimental evidence that construction of the royal chamber is controlled by a pheromone

Significance

Termite mounds are the result of the collective behavior of termites working to modify their physical environment, which in turn affects their behavior. During mound construction, environmental factors such as heat flow and gas exchange affect the building behavior of termites, and the resulting change in mound geometry in turn modifies the response of the internal mound environment to external thermal oscillations. Our study highlights the principles of self-organized animal architecture driven by the coupling of environmental physics to organismal behavior and might serve as a natural inspiration for the design of sustainable human architectures.

Author contributions: S.A.O., A.H., and L.M. designed research, performed research, analyzed data, and wrote the paper.

The authors declare no conflict of interest.

This article is a PNAS Direct Submission.

[1]S.A.O. and A.H. contributed equally to this work.

[2]To whom correspondence should be addressed. Email: lmahadev@g.harvard.edu.

This article contains supporting information online at www.pnas.org/lookup/suppl/doi:10.1073/pnas.1818759116/-/DCSupplemental.

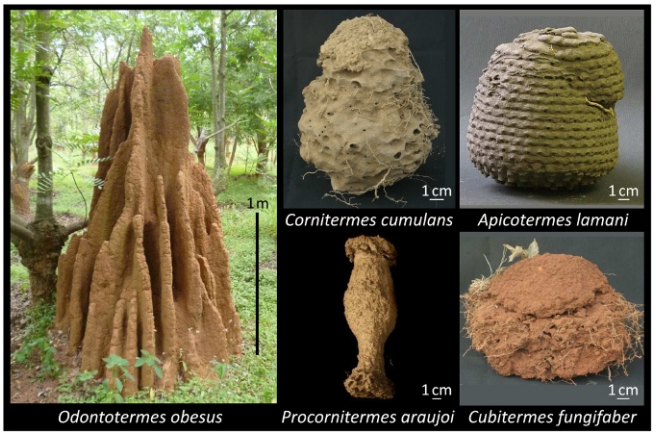

Fig. 1. Variation in natural termite mound morphologies. Photographs show a sample of termite mounds representative of those constructed by five millimetric fungus-harvesting species, labeled at the bottom. *Cornitermes cumulans* and *Cubitermes funifaber* images courtesy of Christian Jost (Centre de Biologie Intégrative, Toulouse, France). *Apicotermes lamani* and *Procornitermes araujoi* images reprinted with permission from ref. 29.

field emitted by the queen, such as chambers and overall mound shape (20). At a similarly large scale, carbon dioxide gradients may be used as templates in nest construction (21). There is, however, only scarce evidence that building pheromones are relevant outside of their influence on the construction of smaller-scale structures including pillars and walls (22).

Here, we present a model for termite mound morphogenesis that results only from the collective behavior of termites acting on local information, yet generates distinctive morphologies resulting from the interplay of physical and behavioral parameters. Our model allows us to explore the potential range of mature mound morphology in terms of a limited number of parameters and also yields simple scaling relationships for mound size, shape, and construction time. Using numerical simulations of the governing equations over a wide range of feasible natural conditions, we follow the geometric variation in mound shapes and see that they are consistent with our scaling predictions as well as naturally observed variation in mound morphology.

Mathematical Model of Mound Morphogenesis

Our fundamental premise is that the shape of a mound results from the collective behavior of termites simultaneously acting on and modifying locally changing information. We characterize this process as a simple feedback loop of physical and behavioral dynamics (Fig. 2), an elaboration of the qualitative theories of past work (20, 23). An incipient developing mound structure determines the flow of heat and air within the mound, which are driven by external temperature oscillations. Internal airflows then transport odor concentrations generated at the mound nest throughout the mound interior (24). This odor field can represent secreted pheromones, metabolic gases such as carbon dioxide, or any other information-carrying particle that can undergo diffusion and advection within the mound. Termite workers adjust their construction behavior in response to local odor concentration and modify the mound structure, completing the feedback loop. This system governs the dynamics of mound morphogenesis until a mature mound size and shape are obtained.

Within the mound environment, our model defines four disjoint subdomains, which are (*i*) the mound interior, which is macroporous; (*ii*) the ground, which consists of the space below a specified ground level that is not part of the mound interior; (*iii*) the surrounding air, which consists of the space above the ground level that is not part of the mound interior or wall; and (*iv*) the wall, the boundary between the interior and the air with a fixed thickness. In addition, we assume that the termite nest is at ground level along the radial center of the mound interior; changing the depth of the nest simply rescales the vertical dimension of the mound. For geometric and numerical simplicity, we limit ourselves to the consideration of axisymmetric mounds.

In these domains, we model the evolution of temperature, airflow, and odor fields as fluids in a porous medium (25). The temperature in the mound $T(\mathbf{r}, t)$ varies due to thermal conduction and fluid convection; heat diffuses within the mound interior and wall with constant thermal diffusivity D_T and is advected by an airflow field $\mathbf{u}(\mathbf{r}, t)$ with an advection weight ν, according to the advection–diffusion equation

$$\frac{\partial T}{\partial t}(\mathbf{r}, t) = \nabla \cdot \left[D_T \nabla T(\mathbf{r}, t) - \nu\, \mathbf{u}(\mathbf{r}, t) \cdot T(\mathbf{r}, t) \right]. \qquad [1]$$

The advection weight ν parameterizes the relative speed at which heat follows the airflow within the mound, and of particular interest is the thermal conduction limit $\nu \to 0$, in which conduction dominates convection. At the interface between the mound wall and air, the temperature fluctuates according to a driving diurnal oscillation set by the mound boundary with the ambient air:

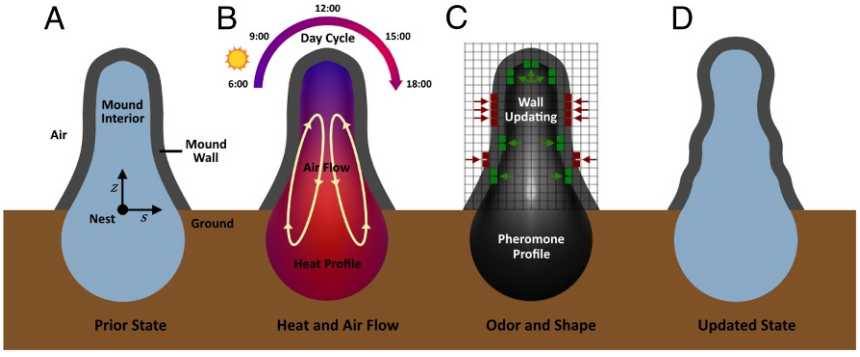

Fig. 2. Schematic of model procedures over a single iteration. (*A*) The previous mound state is composed of disjoint mound regions. (*B*) As the ambient temperature oscillates over a 1-d cycle, the heat profile and airflow field are calculated in the mound interior. (*C*) The odor profile is computed, and the mound wall shape is updated accordingly. Green or red cells indicate sites with an average odor level sufficiently above or below (respectively) the odor threshold, resulting in termites extending the mound outward or allowing the wall to collapse inward. (*D*) The mound shape is updated and used for the next iteration. This process is repeated until convergence to a steady-state morphology.

$$T(\mathbf{r}, t) = \Delta T \sin(2\pi t/\tau), \quad [2]$$

where ΔT is the amplitude of thermal oscillation and τ is the day length. We model the airflow field $\mathbf{u}$ as being driven by heat gradients, following Darcy's law with a conserved fluid,

$$\mathbf{u}(\mathbf{r}, t) = \frac{\kappa(\mathbf{r})}{\eta}\left[\alpha\rho g T(\mathbf{r}, t)\hat{z} - \nabla P(\mathbf{r}, t)\right], \quad \nabla \cdot \mathbf{u}(\mathbf{r}, t) = 0, \quad [3]$$

where $P(\mathbf{r}, t)$ is fluid pressure, $\kappa(\mathbf{r})$ is permeability, η is viscosity, and $\alpha\rho g$ is the buoyancy parameter, with α the thermal expansion coefficient. We take permeability to be a positive constant κ_0 in the mound interior, and zero in the wall and ground.

We model the odor concentration field $\phi(\mathbf{r}, t)$ in the mound as the consequence of small particle diffusion and advection by airflows, with odor production at rate J at the nest. For a central nest at ground height, the odor dynamics follow

$$\epsilon\frac{\partial\phi}{\partial t}(\mathbf{r}, t) = \nabla \cdot \left[D(\mathbf{r})\nabla\phi(\mathbf{r}, t) - \mathbf{u}(\mathbf{r}, t) \cdot \phi(\mathbf{r}, t)\right] + J\delta(\mathbf{r}), \quad [4]$$

where ϵ sets the time scale of the dynamics, $D(\mathbf{r})$ is the odor diffusivity, and $\delta(\mathbf{r})$ denotes the Dirac distribution representing a point source of odor at the nest. We set the odor diffusivity to a positive constant D_0 in the mound interior and the wall and zero in the ground. To impose boundary conditions, we require that the odor concentration vanishes at the edge of the mound, so that $\phi = 0$ outside of the mound. Under the assumption that odor particles are small and highly diffuse, we consider the limit of $\epsilon \to 0$, so that at any point in time, the odor field is a steady-state solution to a rapid advection–diffusion process. This allows the odor field to respond immediately to modifications in the airflow within the mound.

To update the mound morphology iteratively, we suppose that in any local region of the mound wall with an odor concentration above the threshold ϕ_c, termite workers work to enlarge the mound, extending outward the mound boundary. Similarly, in any region along the wall with an odor concentration below ϕ_c, termites no longer maintain the area, and so the mound boundary moves inward due to natural decay. We note that, in this model, the effect of any localized building pheromone or local stigmergic rule will modify the value of ϕ_c. This then represents a general iterative strategy to solve for the steady-state mound shape, which could also emerge from alternative update rules.

For model simplicity, we update the mound geometry only along the boundary and do not model changes in internal structure. As a result, we do not impose conservation of building material as a constraint, as the flux of material between the mound wall and mound interior or exterior is not known. At each update, the below-ground portion of the mound interior becomes a hemisphere having the same radius as the mound at ground level. We assume that the characteristic time for mound construction is long compared with the diurnal time scale; the update frequency is taken to approximately represent a day, while the full construction process can require a month to a year before a steady-state morphology is achieved.

Eqs. **1**–**4** along with the behavioral rules described above complete the prescription of our model and allow us to solve for $T(\mathbf{r}, t)$, $\mathbf{u}(\mathbf{r}, t)$, $\phi(\mathbf{r}, t)$ over a diurnal period τ, and then update these fields before iterating the process. The model has four length scales: (*i*) the wall thickness, h, which for most naturally occurring mounds falls within a narrow range (*SI Appendix*, Table S1); (*ii*) the thermal diffusion length, $L_T = \sqrt{\tau D_T}$, which sets the penetration depth of the diurnal temperature oscillations; (*iii*) the Peclet length of odor, $L_0 = D_0\eta/(\kappa_0\alpha\rho g\Delta T)$, which defines the length scale over which odor diffuses due to buoyancy-driven flow; and (*iv*) a characteristic mound radius, R_c, defined below.

By comparing the characteristic mound radius to the other length scales, we obtain three dimensionless parameters: the Peclet number ($\mathrm{Pe} = R_c/L_0$), the ratio of the characteristic mound radius to the Peclet length of odor; the relative thickness ($\mathrm{Th} = h/R_c$), the ratio of wall thickness to the characteristic mound radius; and the Biot number ($\mathrm{Bi} = L_T/R_c$), the ratio of the thermal diffusion length to the characteristic mound radius, which together define the morphogenetic processes defining steady-state mound shapes.

Although a rough estimate for the Peclet number Pe could be obtained under the assumption of simple molecular diffusion, we explore a wide range of values that give rise to a variety of mound forms. We note that natural pheromones yield typically low Prandtl numbers, and a further reduction to the effective Prandtl number is due to thermal conduction through the mound material and internal air. To reflect this, we consider the thermal conduction limit of small ν, such that thermal Peclet length greatly exceeds the Peclet length of odor.

Using the length scales for characteristic mound radius, thermal diffusion length, and wall thickness as constrained by experiments and natural observations, we find that Peclet numbers are in the range $\mathrm{Pe} \in [10^{-6}, 10^{6}]$, Biot numbers fall in the narrower range $\mathrm{Bi} \in [10^{-2}, 1]$, and the relative thickness lies within the range $\mathrm{Th} \in [10^{-3}, 10^{-1}]$ (*SI Appendix*, Table S1). Variation between natural populations in any of these dimensionless parameters can explain large disparities in mound size and shape observed in nature.

Scaling of Mound Size, Shape, and Construction Time

The natural scaling relationships in our model formulation lead to simple predictions for the size, shape, and construction time of a mature mound. The surface area of the mound at steady state, for example, must be precisely large enough to balance J, the volumetric flux of odor generation inside the mound, with the rate at which odor diffuses out through the mound walls. This outward rate is the product of the total amount of odor within the mound wall Φ, and the characteristic speed at which this odor escapes through the wall is D_0/h. The amount of odor at the mound wall is proportional to $\Phi \sim R^2\phi_c$, since the surface area scales as the squared mound radius R^2 and the average odor concentration at the wall must be precisely ϕ_c, the odor threshold, if steady state is achieved. Hence, we have the relationship $J = R^2\phi_c D_0/h$. Therefore, the mature mound radius at steady-state R_c, i.e., the characteristic mound radius used in our definition of the dimensionless parameters, is

$$R_c \sim \sqrt{\frac{Jh}{D_0\phi_c}}. \quad [5]$$

When the Peclet number is small such that the mature mound approximates a hemisphere, the mature surface area is simply proportional to R_c^2, and so the construction time until the mound converges to its mature size scales as R_c^2/D_T. This represents the time at which the thermal diffusion length L_T matches the steady-state mound radius. Hence, the dimensionless construction time t_c follows the scaling law

$$t_c \sim \frac{R_c^2}{D_T\tau} \sim \mathrm{Bi}^{-2}. \quad [6]$$

A similar scaling prediction can be generated for the mound aspect ratio H/R, the ratio of height H, and radius R of the mound at steady state. This aspect ratio is determined primarily by the convection of odor by vertical air currents, quantified by the Peclet number Pe. An estimate can be obtained by a perturbation approach (*SI Appendix*). The resulting scaling law is

simple: When $\mathrm{Pe} = 0$, diffusion entirely dominates advection, giving rise to a hemispherical mound with a 1:1 aspect ratio, and any deviation in the aspect ratio from perfect sphericity then scales as the squared Peclet number:

$$\frac{H}{R} \sim 1 + \mathrm{Pe}^2, \qquad [7]$$

where the constant of proportionality depends on the other parameters in the model—namely, the Biot number Bi and the relative thickness Th. Hence, the mature mound shape responds quadratically to modification of the Peclet number, as this affects the degree to which air currents transport odor vertically in the mound and promote mound construction and maintenance far above the nest.

In combination, these three simple scaling laws predict a relationship between size, shape, and construction time of natural mounds. Smaller mounds of low R_c, such as those built by termites of the *Cornitermes* genus, will tend to have smaller Peclet numbers and, hence, a more spherical shape, as well as larger Biot numbers and, hence, a shorter construction time. In contrast, the large, meter-sized mounds of high R_c built by some termite species including *O. obesus* will tend to be more elongated and will require longer construction time, assuming similar values for h, L_T, and L_0. In this way, the size, shape, and construction time of natural mounds can be related by the physical parameters that govern the process of mound morphogenesis.

Numerical Simulations of Mound Morphospace

To go beyond the approximate scaling laws for the mature mound radius, surface area, construction time, and aspect ratio derived in the previous section, we now turn to numerical simulations of model Eqs. **1**–**4** solved by using a finite difference model in Matlab. We conducted 500 independent simulations of mound morphogenesis across a wide volume of parameter space representative of the range of feasible natural conditions under which our model can operate, with typical values used to determine the center of each range (*SI Appendix*, Table S1). Each simulation was initialized with a nest encased in a spherical mound wall of fixed thickness and run until a stable steady-state morphology was obtained, and the dynamic size and shape of each mound was tracked over time (Fig. 3 and Movie S1). Because our model has no cylindrically asymmetric effects, all simulated mounds must preserve their cylindrical symmetry over time, so we integrate the morphogenesis model by discretizing in cylindrical coordinates.

While sweeping through each of the full range of dimensionless parameter values assumed in our model formulation, we measured mound size and shape after convergence to a steady-state morphology, which occurred between 5 and 500 iterations after initialization. Using mound volume as a measurement of mound size, and using aspect ratio and mound sphericity (the ratio of the surface area of a sphere to the surface area of the mound, proportionally scaled to range between 0 and 1) as measurements of mound shape, we tested for relationships between mound morphology and the three dimensionless parameters that control the system.

Within the large volume of searched feasible parameter space (Fig. 4), our simulations found that mounds with low relative thickness and low Biot number tend to grow to larger volumes. Indeed, by definition, these two dimensionless quantities should be relatively small when the critical mound radius is large. Moreover, we found that mound sphericity was strongly promoted by low Peclet number, while high Peclet numbers resulted in more unusual, aspherical mound shapes. This confirms our intuition that systems with high Peclet numbers, where convective currents dominate conduction, can grow in a focused direction due to the airflow transporting the odor in the direction of growth. The nonlinear and nonmonotonic nature of these associations was evident both in parameter space and when steady-state mound shapes were plotted on size–shape axes that define a mound morphospace (*SI Appendix*, Fig. S2). However, despite the simplicity of our model, there exists no simple relationship between mound size and Peclet number, nor does mound shape appear to be strongly affected by either relative thickness or Biot number within the parameter range tested.

We found that the simulated mound morphologies conformed well to our simple scaling predictions across the full range of plausible model parameters (Fig. 5).

Discussion: Physics, Behavior, and Architecture

Termite mounds are one of the most remarkable examples of self-organized animal architectures, and the range of shapes and sizes that they exhibit have excited the imagination of scientists for a long time (9). To explain these morphologies, we provide a simple, coarse-grained theory that couples the physics of heat and mass transport to termite building behavior. The resulting morphology then feeds back on the transport processes until a dynamic steady state is achieved. This two-way coupling between termite behavior and local temperature and airflow suffices to generate a variety of mound geometries as three dimensionless

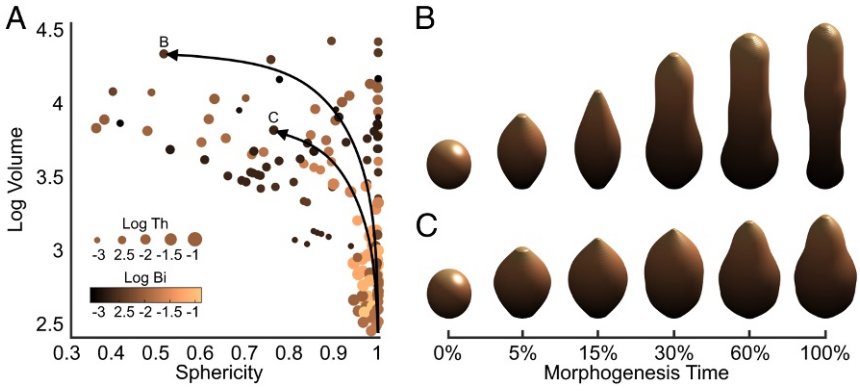

Fig. 3. Morphogenesis dynamics of simulated mounds. (*A*) Various steady-state mound morphologies are plotted in a 2D morphospace of mound sphericity and $\log_{10}$ volume, relative to the critical mound radius. Points are colored and sized by the Bi and Th values used in the simulation. The two black trajectories show two possible paths through this morphospace, from an initially small and spherical mound to the mature shape. (*B* and *C*) Progression of mound geometries during morphogenesis. Each row corresponds to a single mound as it progresses along the corresponding trajectory in *A*. Parameters were set to $\mathrm{Bi} = 10^{-2}$, $\mathrm{Th} = 10^{-2}$, and $\mathrm{Pe} = 4 \times 10^4$ (*B*) or $\mathrm{Pe} = 2 \times 10^2$ (*C*).

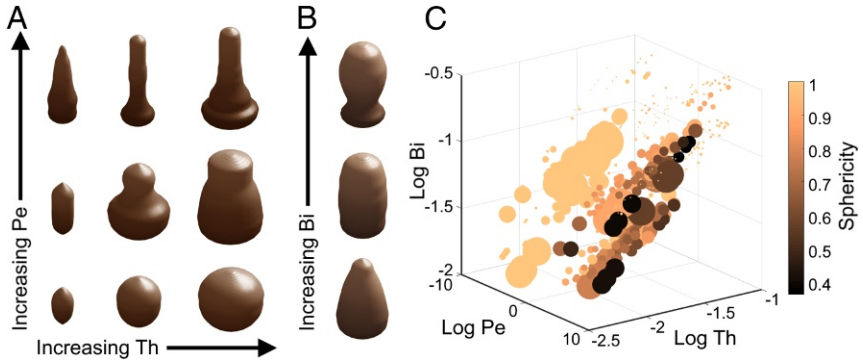

Fig. 4. Mapping model parameters to mature mound morphologies. (*A*) An array of nine simulated mound shapes for varying relative thickness Th and Peclet number Pe, for fixed Biot number Bi = 0.05. (*B*) Three simulated mound shapes for varying Bi for fixed Th = 0.05 and Pe = 200. (*C*) Dimensionless parameter space of our morphogenesis model. Each dot corresponds to a single simulation, with dot position giving the values of Pe, Th, and Bi from the simulation, dot size proportional to the mound volume at steady state, and dot color corresponding to mound sphericity at steady state according to the color bar. Axes represent base-10 logarithms of the dimensionless model parameters.

parameters characterizing the geometry and dynamics of heat and fluid transport are varied.

In the absence of any existing field experiments to compare with, we ask whether the variability of mound morphologies as a function of species and climates around the world is qualitatively consistent with our model. The growth of mounds is dominated by building processes at the surface and limited by molecular diffusion of pheromones through the mound wall. As a mound grows, unless more termites are recruited into the building process, the volumetric density of termites decreases over time. Nevertheless, larger termite colonies should build larger mounds, as has been observed within and across many termite taxa, including *Nasutitermes*, *Macrotermes*, and much of the *Termitinae* subfamily (26). Our model agree with this intuitive relationship, as larger colonies will tend to produce a greater quantity of odor, and this high rate J will result in a large mound radius R_c.

Moreover, our model agrees with the simple intuition that larger mounds will take longer to construct, and, as a result, the distribution of mounds in an area may be more sparse than smaller mounds, which can be constructed quickly and may be quite dense. This relationship aligns with the observation that large *Macrotermes* mounds have a low density of 1–4 ha^{-1} (27), while small *Cubitermes* mounds have a substantially higher density of 385–496 ha^{-1} (28). Our results also show that, cetus paribus, the absolute size of termite mounds increases with the amplitude of temperature oscillations. Consistent with this, the mounds of the genus *M. michaelseni* found in the open grasslands of southern Africa are much taller than those of the genus *O. obesus* from the subtropical grasslands and forests of south

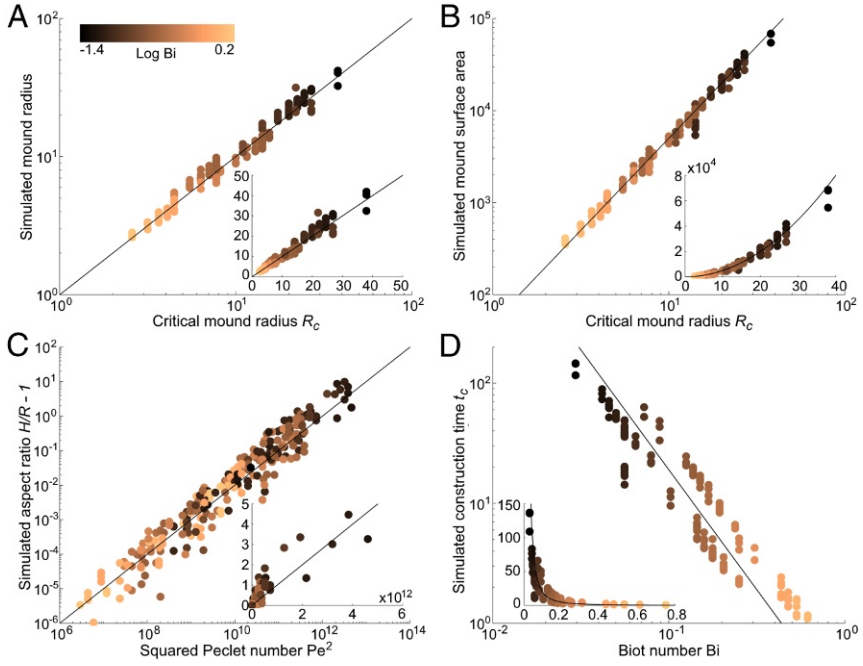

Fig. 5. Correspondence between analytical scaling predictions and simulated mature mound morphologies. (*A*) Simulated mound radii are well predicted by the critical mound radius R_c as defined in the main text. (*B*) Mound surface area grows approximately in proportion to the square of R_c. (*C*) The mound aspect ratio H/R scales as $1 + Pe^2$, where Pe is the Peclet number. (*D*) The construction time t_c until the mound achieves its mature size scales approximately as the inverse-squared Biot number Bi. All axes have been scaled by the appropriate proportionality factors, and all points are colored according to the base-10 logarithm of the Biot number (Bi).

Asia, as the scale of diurnal temperature oscillations in covered forests are mitigated by the shade (8). In our proposed modeling framework, it is these diurnal thermal oscillations that provide the external fluctuations that drive the mound-construction process, as opposed to external pressure gradient or wind flow. This choice was informed by previous studies on the external conditions that induce interior transient flows in the termite mounds of *O. obesus* (7) and *M. michaelseni* (8). In the mounds of both species, external wind was found to play a subordinate role relative to the dominant thermal mechanism considered by our model in this work.

The modeling framework presented here suggests several possible extensions, each at the expense of model simplicity. Currently, our model does not address changes in mound shape associated with mechanical forces and mound settling under the influence of gravity, a process that is likely important during the early stages of mound building. Furthermore, the current model averages over the complex internal structure of the mound, clearly seen in excavated nests and captured in agent-based simulations (16, 29). These labyrinthine structures change the detailed mechanics of heat and mass transport while also making these processes heterogeneous, effects that will lead to fluctuations in the shape and stability of the mound. The construction of these internal nest structures in social insects has already seen modeling interest (17–19). Instead, by averaging over these complex internal structures, our continuum model serves to provide a global picture of the generation of the overall mound form.

Our coarse-grained macroscopic model could serve as the outer problem that drives and is driven by the microscale processes at the level of individual agents. For example, we have neglected here the effects of active transport of water by termites within the mound and the passive dynamics of evaporative cooling that will change the temperature profiles and thereby the mechanics of odor transport. Moreover, our threshold-based update rule gives rise to one possible set of dynamics leading to an equilibrium mound form, and it serves to roughly capture the idea that termite workers respond to the odor in a sensitive manner by shaping their environment. The incorporation of more nuanced individual behaviors or other nonthresholded update rules, including a linear relationship between local odor concentration and worker activity, could result in altered dynamics, although the properties of our system would nonetheless lead the mound to converge upon the same equilibrium morphology.

Finally, the radially symmetric formulation of our morphogenesis model adequately captures the largely symmetric shapes of natural mounds, but clearly neglects a few potential sources of asymmetry. We assume that the termite nest is approximately positioned along the central mound axis at ground level, although asymmetric or subterranean nests can alter the odor dynamics and lead to different, radially asymmetric steady-state mound shapes. Consistent bias in directed sunlight may also be a source of radial asymmetry, yielding effects such as the northward tilt seen in mounds of *M. michaelseni* in the Southern Hemisphere (30). Likewise, fluctuations in the direction of sunlight may lead to cyclic asymmetric growth on the time scales of days and years, which may be particularly relevant to understanding mound morphogenesis far from the Equator [for example, in Australian compass termites (5)].

Generalizing our model to account for these additional effects is certainly within the realm of possibility and would be important to address the ecological and evolutionary aspects of mound morphogenesis. Furthermore, understanding similar principles underlying the construction of animal architectures such as ant nests and beehives are natural next steps, as are quantitative predictions of our theory in specific contexts such as mound repair and maintenance. More broadly, our theory demonstrates how an organism capable of building behavior can respond to its macroenvironment by changing its microenvironment, via a feedback process leading to a nonequilibrium steady state that is adaptable and robust by virtue of this feedback loop. This is clearly not limited to social insect architecture. Indeed, we humans do it all of the time; as W. Churchill pointed out a long time ago, "We shape our buildings; thereafter they shape us."

ACKNOWLEDGMENTS. We thank H. King for helpful discussions. Partial support was provided by NSF Graduate Fellowship DGE 1144152 (to A.H); the Human Frontiers Science Program under Grant RGP0066/2012-TURNER (to S.A.O. and L.M.); the Henry W. Kendall Physics Fellowship (S.A.O.); the Karel Urbanek Applied Physics Fellowship (S.A.O.); the MacArthur Foundation (L.M.); and NSF Physics of Living Systems Grant PHY1606895 (to L.M.).

1. Korb J (2001) Termite mound architecture, from function to construction. *Biology of Termites: A Modern Synthesis*, eds Bignell DE, Roisin Y, Lo N (Springer, Dordrecht, The Netherlands), pp 349–373.
2. Korb J (2007) Termites. *Curr Biol* 17:R995–R999.
3. Heinrich B (1981) *Insect Thermoregulation* (Wiley-Interscience, New York).
4. Korb J (2003) Thermoregulation and ventilation of termite mounds. *Naturwissenschaften* 90:212–219.
5. Jacklyn PM (1992) "Magnetic" termite mound surfaces are oriented to suit wind and shade conditions. *Oecologia* 91:385–395.
6. Cosarinsky MI (2011) The nest growth of the neotropical mound-building termite, *Cornitermes cumulans*: A micromorphological analysis. *J Insect Sci* 11:122.
7. King H, Ocko S, Mahadevan L (2015) Termite mounds harness diurnal temperature oscillations for ventilation. *Proc Natl Acad Sci USA* 112:11589–11593.
8. Ocko SA, et al. (2017) Solar-powered ventilation of African termite mounds. *J Exp Biol* 220:3260–3269.
9. Hansell M (2005) *Animal Architecture* (Oxford Univ Press, Oxford).
10. Grassé P-P (1959) Reconstruction of the nest and coordination between individuals in terms. *Bellicositermes natalensis* and *cubitermes* sp. the theory of stigmergy: Test interpretation of termite constructions. *Soc Insect* 6:41–80.
11. Theraulaz G, Bonabeau E (1999) A brief history of stigmergy. *Artif Life* 5:97–116.
12. Camazine S, et al. (2001) *Self-Organization in Biological Systems* (Princeton Univ Press, Princeton).
13. Theraulaz G, Bonabeau E (1995) Coordination in distributed building. *Science* 269:686–688.
14. Bonabeau E (1997) From classical models of morphogenesis to agent-based models of pattern formation. *Artif Life* 3:191–211.
15. Courtois PJ, Heymans F (1991) A simulation of the construction process of a termite nest. *J Theor Biol* 153:469–475.
16. Khuong A, et al. (2016) Stigmergic construction and topochemical information shape ant nest architecture. *Proc Natl Acad Sci USA* 113:1303–1308.
17. Deneubourg JL (1977) Application de l'ordre par fluctuations à la description de certaines étapes de la construction du nid chez les termites. *Insect Soc* 24:117–130.
18. Bonabeau E, et al. (1988) A model for the emergence of pillars, walls and royal chambers in termite nests. *Phil Trans R Soc B* 353:1561–1576.
19. Franks NR, Deneubourg JL (1997) Self-organizing nest construction in ants: Individual worker behaviour and the nest's dynamics. *Anim Behav* 54:779–796.
20. Bruinsma OH (1979) An analysis of building behaviour of the termite *Macrotermes subhyalinus* (Rambur). PhD dissertation (Wageningen University and Research, Wageningen, The Netherlands).
21. Cox MD, Blanchard GB (1977) Gaseous templates in ant nests. *J Theor Biol* 204:223–238.
22. Fouquet D, Costa-Leonardo AM, Fournier R, Blanco S, Jost C (1977) Coordination of construction behavior in the termite *Procornitermes araujoi*: Structure is a stronger stimulus than volatile marking. *Insect Soc* 61:253–264.
23. Howse PE (1966) Air movement and termite behaviour. *Nature* 210:967–968.
24. Darlington J, Zimmerman P, Greenberg J, Westberg C, Bakwin P (1997) Production of metabolic gases by nests of the termite *Macrotermes jeanneli* in Kenya. *J Trop Ecol* 13:491–510.
25. Bear J (2013) *Dynamics of Fluids in Porous Media* (Courier Corporation, North Chelmsford, MA).
26. Josens G, Soki K (2010) Relation between termite numbers and the size of their mounds. *Insect Soc* 57:303–316.
27. Pomero DE (1977) The distribution and abundance of large termite mounds in Uganda. *J Appl Ecol* 14:465–475.
28. Ferrar P (1982) Termites of a South African savanna. II. Densities and populations of smaller mounds, and seasonality of breeding. *Oecologia* 52:133–138.
29. Perna A, Theraulaz G (2017) When social behaviour is moulded in clay: On growth and form of social insect nests. *J Exp Biol* 220:83–91.
30. Turner JS (2000) Architecture and morphogenesis in the mound of *Macrotermes michaelseni* (Sjöstedt) (Isoptera: Termitidae, Macrotermitinae) in northern Namibia. *Cimbebasia* 16:143–175.

Supporting Information

Ocko et al.

Supporting Tables and Figures

Table S1. Table of quantities and associated units.

Quantity	Symbol	Units	Typical Values
Thermal amplitude	ΔT	Temperature	$4°$C
Day length	τ	Time	24 hours
Thermal diffusivity	D_T	Distance^2/Time	19 mm^2/sec
Mound permeability	κ_0	Distance^2	10^{-4} mm^2
Odor production rate	J	Concentration/Time	10 ng/hour
Odor diffusivity	D_0	Distance^2/Time	125 μm^2/sec
Odor threshold	ϕ_c	Concentration	0.15 mg/μm^3
Wall thickness	h	Distance	35 mm
Relative thickness	Th	Dimensionless	$10^{-3} - 10^{-1}$
Biot number	Bi	Dimensionless	$10^{-2} - 1$
Peclet number	Pe	Dimensionless	$10^{-6} - 10^{6}$

Movie S1. See supplemental video file for six 3D rendered animations of simulated termite mounds undergoing morphogenesis. All mounds were initialized as a small sphere and allowed to grow until a steady state morphology was obtained. Parameter value are given before each animation in log10 scale. Each frame corresponds to one day of mound growth, such that the length of each animation in frames is equal to the construction time of the mound.

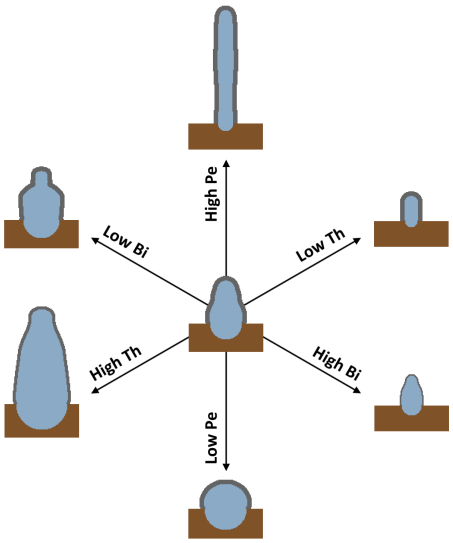

Fig. S1. Example of the qualitative effects of altering the model parameters on the steady-state mound shape. The mound in the center is produced when Pe $= 1$, Bi $= 0.05$, Th $= 0.007$. Each arrow corresponds to a tripling or thirding of a single dimensionless quantity, with all other parameters held constant.

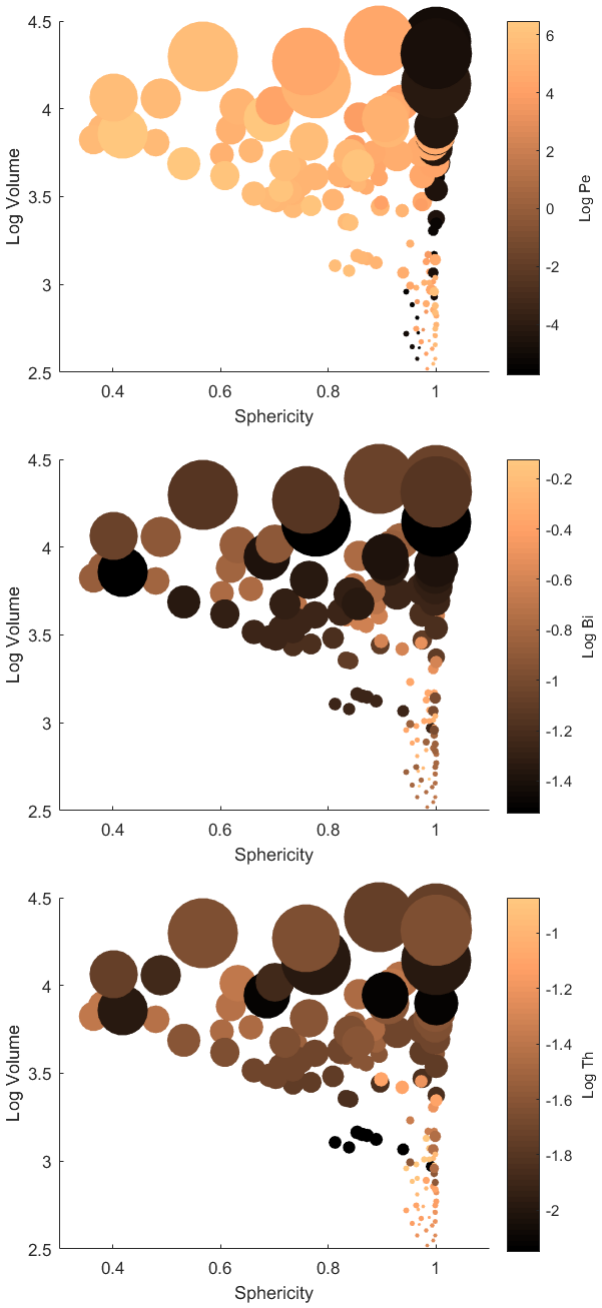

Fig. S2. Mound morphospace, defined at steady state by mound sphericity in the horizontal direction and log mound volume, measured relative to the critical mound radius, in the vertical direction. Each dot corresponds to a single simulation. Dot position indicates mound shape and size, and dot color corresponds to each of the three dimensionless quantities in the model, top: Pe, center: Bi, bottom: Th. Dot size is proportional to the absolute steady-state mound volume, and nest depth was set to zero for all simulations.

Perturbation Theory for Mound Aspect Ratio

To derive the scaling prediction (equation 7 of the main text) for the mature mound aspect ratio H/R, we use a perturbation approach. The steady state advection-diffusion equation (equation 4 of the main text) can be solved for the odor concentration $\phi(\mathbf{r},t)$ in the form of a Taylor expansion in the Peclet number,

$$\begin{aligned}\phi(\mathbf{r},t) = \phi_0(\mathbf{r}) + \mathrm{Pe}\,\phi_1(\mathbf{r})\big\{\Delta T(\mathbf{r}',t)\big\} \\ + \mathrm{Pe}^2\phi_2(\mathbf{r})\big\{\Delta T(\mathbf{r}',t),\Delta T(\mathbf{r}'',t)\big\} + O(\mathrm{Pe}^3),\end{aligned} \quad [S1]$$

where ϕ_0 is the solution when $\mathrm{Pe}=0$, and ϕ_1 and ϕ_2 are first- and second-order perturbations that are linear and quadratic functionals of ΔT. The average odor field $\bar{\phi}(\mathbf{r})$ over one full day can be calculated with an integral which may be symmetrized:

$$\bar{\phi}(\mathbf{r}) = \frac{1}{\tau}\int_0^{\tau}\phi(\mathbf{r},t)\,dt = \frac{1}{\tau}\int_0^{\tau/2}\Big[\phi(\mathbf{r},t)+\phi(\mathbf{r},t+\tfrac{\tau}{2})\Big]dt. \quad [S2]$$

Substituting (1) into (2), we can exploit symmetry in the day-night cycle using $\Delta T(\mathbf{r},t) = -\Delta T(\mathbf{r},t+\frac{\tau}{2}) + O(\mathrm{Pe}^2)$, such that the first order terms precisely balance, while the second order terms sum to give upon simplification the result

$$\bar{\phi}(\mathbf{r}) \approx \phi_0(\mathbf{r}) + \frac{\mathrm{Pe}^2}{\tau}\int_0^{\tau}\phi_2(\mathbf{r})\big\{\Delta T(\mathbf{r}',t),\Delta T(\mathbf{r}'',t)\big\}\,dt, \quad [S3]$$

where the approximation arises from neglecting terms beyond second order. Note that two perturbations of order Pe^2 arise, one coming from heat advection, and the other from odor advection; here we work in the limit of low Prandtl number.

When $\mathrm{Pe}=0$, the mound aspect ratio H/R must be equal to one, and any slight perturbation to $\bar{\phi}$ will create a proportional perturbation to the aspect ratio. From this we obtain the scaling prediction

$$\left(\frac{H}{R}-1\right) \propto \Delta\bar{\phi}(\mathbf{r}) \propto \mathrm{Pe}^2 \quad [S4]$$

where the constant of proportionality depends on the other parameters in the model, namely the Biot number Bi and the relative thickness Th. This can then be written as the scaling prediction $(H/R) \sim 1 + \mathrm{Pe}^2$, as reported in the main text.